Available online at www.sciencedirect.com

ScienceDirect

journal homepage: http://www.elsevier.com/locate/acme

Original Research Article

Modelling of the material destruction of vertically arranged honeycomb cellular structure

Jarosław Piekło [a], *Marcin Małysza* [b], *Rafał Dańko* [a,*]

[a] *AGH University of Science and Technology, Faculty of Foundry Engineering, Krakow, Poland*
[b] *Foundry Research Institute, Krakow, Poland*

ARTICLE INFO

Article history:
Received 9 August 2017
Accepted 29 March 2018
Available online 01 May 2018

Keywords:
Skeleton castings
Additive manufacturing
Cellular structure
Tensile testing
Numerical analysis
Material destruction modelling

ABSTRACT

The paper presents the results of the experimental and numerical analysis of material destruction of honeycomb cellular structure. Based on the experimental research, the results of numerical calculations regarding the compression process were verified along with the correctness of used constitutive numerical model. The destruction was analyzed for the casting with no structural defects and for the casting with detected porosities. The results were compared to the structural strength of the honeycomb structure manufactured on the CNC machine. The metallic honeycomb structure was manufactured as a casting of Al alloy in the investment casting technology. For manufacturing purposes the honeycomb model was obtained in additive manufacturing process. The castings and the CNC honeycomb were used in the compression test trials. The process was controlled by the displacement and the results were registered as the changes of the height and the force value. Based on the experimental results the numerical model of honeycombs was introduced for the numerical analysis of the energy absorption and compression process. The results showed good correlation between the experiment and FEM (*Finite Element Method*) analysis.

1. Introduction

The use of cellular structure materials in the various fields of technologies is the result of the research of the internal structure of i.e. plants, which shows the optimal combination of two parameters: high strength and low mass [1]. The use of available knowledge in the field of biomechanics has become the basis for designing of cellular structures of metallic, plastic, ceramic and composite materials. The main feature of cellular materials is the presence of internal air or gas filled spaces, voids that reduce their density compared to the solid material. Optimal shapes manufactured from various types of technologies, shows high properties for energy absorption capacity during static and dynamic loading, which makes it possible for the military, aerospace, automotive, and many more industrial applications. A wide range of such materials makes it necessary to systematize them and extract special types of the designing and the manufacturing processes. The basic division of cellular material is based on the void occurrence. The first type is the regular cellular structure with the voids evenly distributed and the second type, irregular cellular structures

* *Corresponding author.*
E-mail addresses: jarekp60@agh.edu.pl (J. Piekło), marcin.malysza@iod.krakow.pl (M. Małysza), rd@agh.edu.pl (R. Dańko).
https://doi.org/10.1016/j.acme.2018.03.007
1644-9665/

where the voids occur randomly. The research on the mechanical behaviour of cellular structure is a very wide issue. The research scope of many publications is to optimize the topology of a single cell in terms of strength to weight ratio, develop the analytical and numerical models, conduct laboratory experiments in order to define the model of destruction and internal coherency during the energy dissipation and perforation under the influence of external force along with the determination of critical values of compression velocities and energy absorption In the field of metal casting the cellular structures can be a part of the skeletal shape of the casting or be used as a component of the casting tooling. In the first case, research work related to manufacturing technology focuses on the use of traditional foundry techniques based on a geometrically complex core and gravity casting using the metallostatic pressure [2,3], or on the use of 3D printing methods to prepare a mould or a foundry model necessary to make a skeleton casting [4]. In the second case, the cellular structure is a part of the tooling used in casting process i.e. high pressure die casting as the element of die cooling system [5]. Cellular structures due to their application are usually subjected to static or dynamic compressive forces, and questions related to the course of their decohesion are the subject of numerous works and publications: [6–8]. The authors of the publication emphasize the importance of the impact of defects that may occur in the cellular structure on the destruction process [3]. In the case of casting structures, the defects are related with shrinkage or gas porosity, the influence of which on the process of decohesion of the structure is, among others, the subject of this work. The possibility to prepare a reliable numerical model based on the material properties allows for testing the cellular structure in various exploitation conditions. Due to that possibility the assumption was taken to conduct analysis of perpendicular loading of the cells on presented cellular structure shape.

2. Design and types of regular cellular structures

According to Ashby and Gibson [9] the cellular structures are described as an interconnected network of solid struts or plates which form the edges and faces of a cell. A typical example of such structure is the honeycomb shape, which is the subject of presented series of analysis. In that shape the plates are connected by the edges forming an elementary hexagonal cell shape. The shapes of the elementary cell could be a simple or very complicated geometries. When the geometries are connected to each other in the certain configuration, with additional connected panels on the bottom and top are creating sandwich type structures. The design of sandwich structure topology is based on the acting external and internal forces and the purpose of the structure. Cellular materials are characterized by a lower relative density Δ compared to the material from which they are made, defined as the density ratio of the porous material ρ_p to the solid ρ_s:

$$\Delta = \frac{\rho_p}{\rho_s} \tag{1}$$

In case of relative density, generally we can use the relationship as:

$\rho_p/\rho_s < 0.3$ – a density ratio where the material can be defined as a cellular structure,

$\rho_p/\rho_s > 0.8$ – a density ratio, where the material only has pores in the structure of the solid material.

Generally the metal in the cellular structure typically is less than 20% of its volume.

3. Manufacturing of the regular cellular structure in the casting methods

In general the manufacturing methods can be divided into [10,11]:

- Shaping in the meanings of plastic processing of prefabricated components and combining them with the laser welding, traditional welding or glueing,
- Methods of investment casting.

In the presented subject the investment casting method was used in the manufacturing process of cellular structures. The model was 3D-printed in the *FDM* technology as additive manufacturing process. An important advantage of *AM* technology is the possibility to obtain very complex geometries. Additionally the practical use of the results of the strength shaping and compression of cellular structure can be visualized. There are some limitations of the *AM* manufacturing technology, which are involved with the minimal wall thickness and the needs of removing of supporting material after printing process. For the casting method there are limitations also regarding the wall thickness of the mould, the flowability of the liquid metal and removal of residues of mould during cleaning of the casting [12]. In the ceramic shell making process as pattern a wax, ABS or different *AM* material can be used. Due to complicated shapes of the cellular structure the alloys with good flowability should be used, for example Al–Si, Cu–Be and some of the super alloys group. The advantage of using casting methods is the possibility to obtain casting structures with complicated internal and external geometries different from the sandwich type structure where the top and bottom closing plates are used. The use of special techniques of casting such as centrifugal or high pressure casting allows for obtaining casting with different amount of casting defects i.e. shrinkage porosity.

The cellular model was designed in the CAD software and exported to the native file to the *FDM* 3D printing machine. The dimensions of the model are 80 mm × 80 mm × 20 mm. In the 3D printing the geometry needs to be divided into layers along with the definition of nozzle path, size and speed. For the model manufacturing a thermoplastic ABS material was used.

Models presented in Fig. 1 were used for the manufacturing of the silicone mould. Specially designed core allows for easy wax patter removal. In Fig. 2 the silicone mould, wax patterns and tree assembly used for the ceramic shell preparation are presented.

The pattern tree was moulded in the plaster with the assist of vacuumed, which was used to obtain good surface quality. The plaster material was moulded in the special sleeve with the

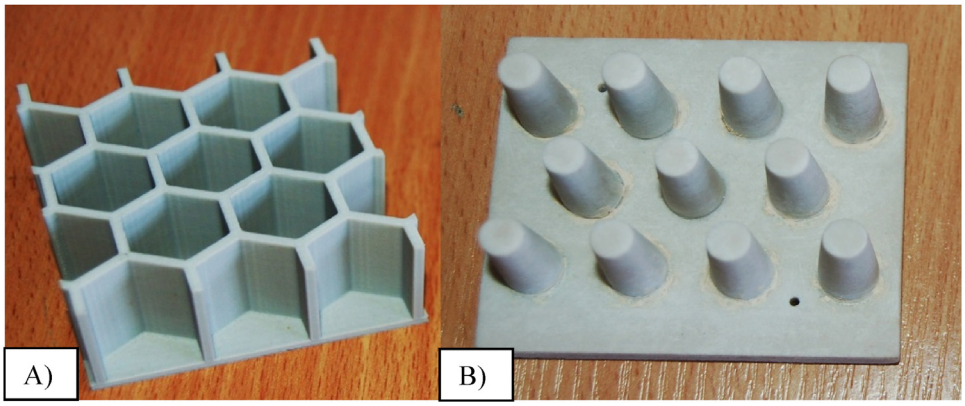

Fig. 1 – (A) Honeycomb shape ABS model, (B) special core used in the wax patterns manufacturing.

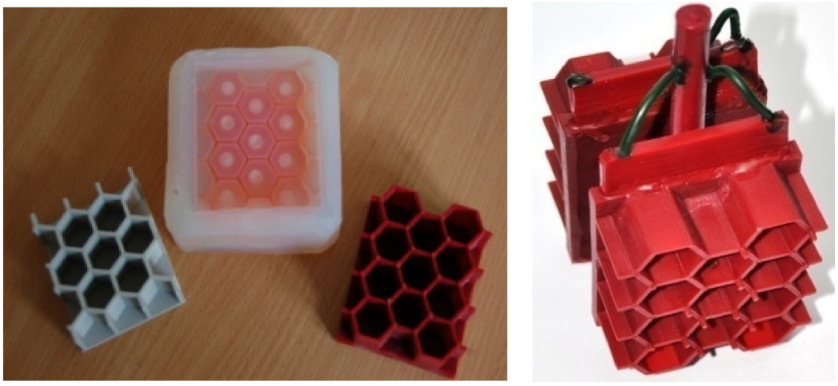

Fig. 2 – Silicone mould and the assembly of wax patterns and gating system.

150 mm diameter. When the plaster was fully bounded the mould was placed in the heating oven for dewaxing and removal of initial moisture. After dewaxing the mould was heat treated to obtain stable temperature in the whole cross-section. Then the heated mould was placed in the special vacuum casting furnace and filled with aluminium alloy with the chemical composition close to 4xxx.0 series alloy in the argon atmosphere with under- pressure of 300 mbar. Final honeycomb casting with the gating system is presented in Fig. 3.

4. Laboratory trials

The development of the numerical model of the deformation of honeycomb structure under the compression force required a series of tensile tests. The chemical composition of the honeycomb structure castings are presented in Table 1. The chemical composition due to melting of scrap material is close to 7xxx.0 and 4xxx.0 series alloys. The laboratory tensile strength testing's was carried out to obtain the mechanical properties of elastic and plastic deformations, and the effect of the triaxiality of the stress state T_R on the relationship between stress and deformation. Tensile strength testing's were performed on the test samples with the 6 mm diameter and notch samples with the notch dimensions of 1; 2; 4 and 7 mm. The dimensions and the shape of a test sample with the notch is presented in Fig. 4.

Conducted laboratory trials of mechanical properties includes the determination of yield strength R_{02}, tensile strength R_m, elongation $A_{2.5}$ and the elastic modulus E. For the notched samples the values for the breaking force F_u,

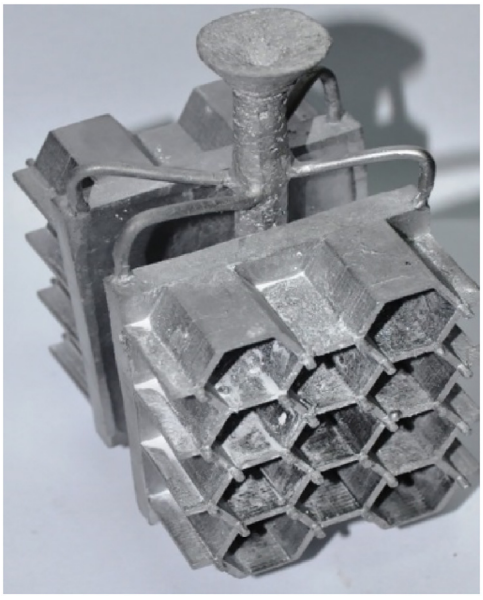

Fig. 3 – Honeycomb structure castings with gating.

Table 1 – Chemical composition of alloys used in the trials.

Alloy type	Zn	Si	Cu	Mg	Ti	Mn	Fe
4xxx.0	0.1	8.5	1.1	0.5	0.11	–	0.05
7xxx.0	4.9	0.5	0.7	3.1	0.1	0.3	0.5

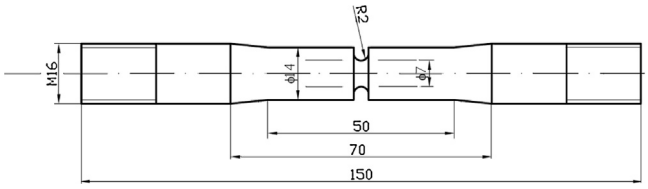

Fig. 4 – The ring shape notch test sample $\rho = 2$ mm, used for determination of the influence of the triaxiality of the stress state on the maximal deformation.

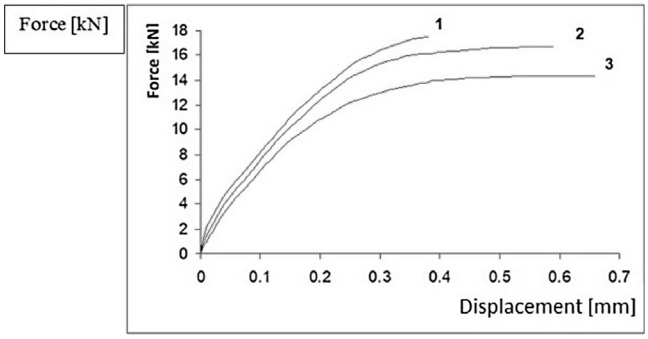

Fig. 5 – The comparison of the tensile analysis of samples with different radius, σ curve 1 – $\rho \equiv 2$ mm, curve 2 – $\rho \equiv 4$ mm, curve 3 – $\rho \equiv 7$ mm for 7xxx.0 alloy.

breaking stress R_u, the deformation ε_u and the value of tensile force as a function of deformation in the notch area.

The results shows that the notch inflicts significantly decrease elongation compared to the results of tensile strength testing. There is also an increase of the breaking force F_u, along with the ring notch radius decreases. Gathered results in the form of a graph presents the change of the force in the function of the deformation of the notch area for different radius for the 7xxx.0 series aluminium alloy. The relationship between the rapture deformation and the degree of the triaxiality of the stress T_R, is determined by the radius and the shape of the notch. The triaxiality of the stress state is characterized by the ratio of the average stress σ_m to the stress intensity σ_{int}: $T_R\sigma_m/\sigma_{int}$ and the stress intensity is described by the Hubera–Misesa–Hencky'go (HMH) hypothesis. The tensor stress components within the notch area are determined by the solution given by the Bridgman [13]. Based on that the triaxiality of the stress can be determined, which can be also calculated based on the numerical analysis of the test samples with different notch radius (Fig. 5).

In Table 2, some mechanical properties of the 7xxx.0 series aluminium alloy for different notch radius along with the sample with $\rho = 0$, are presented. The table presents as well the theoretical triaxiality of the stress state based on the Bridgman's approach T_{Rt}, numerical FEM calculations T_{RHMH}, and the values for conditions of 5% porosities occurrence T_{RGTN}.

The results of the conducted analysis were used for the determination of the behaviour of the material during compression and for the determination of the model describing the initiation of destruction conditions. The laboratory trials were conducted on the cellular honeycomb structure manufactured from the mentioned alloys. The trials were done in the *MTS* mechanical testing machine, where the deformation was induced by the compression force. The results of the compressions are presented in Figs. 6 and 7 respectively. The absorbed energy during compression of the cellular structure was registered in the form of curves of the displacement and forced and used for the evaluation of the numerical model. The results are presented in Figs. 8 and 9.

For the determination of mechanical properties of 4xxx.0 alloy the tensile mechanical test was conducted. The tensile strength curve is presented in Fig. 10. The results were used in the database for determination of material properties in the simulation software.

Additionally the cast honeycomb structure was analyzed for the internal porosities. The visualization of defects analysis is presented in Fig. 11.

The presented image shows the porosities and surface defects of the casting. It has also small amount of noises and slight light overexposure. It is known that all castings have a minimal content of porosities due to the nature of the solidification process. It was stated that for the numerical analysis was assumed 5% of internal porosities.

Table 2 – Mechanical properties of 7xxx.0 series aluminium alloy for different notch samples radius ρ and the triaxiality of the stress state T_R.

Notch radius	The stress at the break point	Deformations at the break point	Theoretical triaxiality of the stress state	Triaxiality of the stress state based n the H–M–H model	Triaxiality of the stress state based on the Gursona model
ρ [mm]	R_u [MPa]	σ_u [%]	T_{Rt}	T_{RHMH}	T_{RGTN}
0	364	3.98	0.33	0.33	0.33
2	455	0.38	0.96	1.01	1.32
4	434	0.59	0.69	0.71	0.81
7	374	0.66	0.55	0.58	0.61

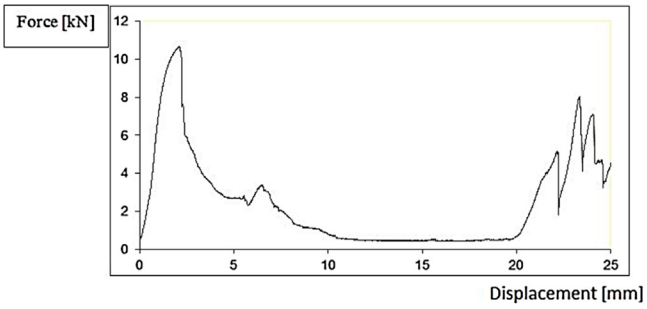

Fig. 6 – The changes of the force value during the compression of the honeycomb structure manufactured from the 4xxx.0 series aluminium alloy in the CNC machining process.

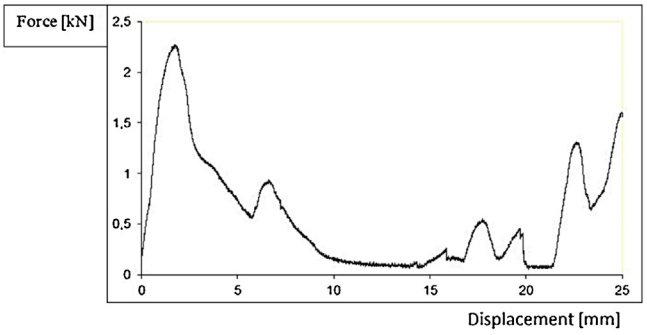

Fig. 7 – The changes of the force value during the compression of the honeycomb structure from the 4xxx.0 series aluminium alloy.

5. Constitutive material modelling

The numerical model of the honeycomb structure compression which is based on the Abaqus software [14], requires precise material definition, since it has the highest influence on the correctness of the results. In addition the definition of the basic properties of the alloy in terms of elastic and plastic deformations, it is necessary to define the criterion of destruction initiation and growth. It was assumed that in the analyzed model, the reduced plastic deformation $\varepsilon_D{}^{pl}$ at the initial time of failure initiation is a function of the degree of triaxial stress T_R:

$$\epsilon_D^{pl} = f(T_R) \tag{2}$$

The criterion of failure initiation is fulfilled when the variable ω_D, which is rising monotonically and its increase the $\Delta\omega$ is computed during each iteration and equals 1;

$$\omega_D = \int \frac{d\epsilon^{pl}}{\epsilon_D^{pl}(T_R)} = 1 \tag{3}$$

It is assumed that the failure occurs during the progressive degeneration of material rigidity leading to its destruction. The significant element which the stiffness is lower than assumed value, can be removed from the model or can only transfer the hydrostatic compression stress (Fig. 12).

The decrease of stiffness of the element starts when the elastic stress reaches the critical value σ_o. From that point the relationship between deformation and real stress is no longer a continuation of the tensile curve (the dotted line), instead the stress value varies according to the equation:

$$\sigma = (1-D)\sigma^* \tag{4}$$

The variable σ^* determines the temporary stress value without the material failure. The damage degree is in the range from 0 to 1. When the $D = 1$, the deformation intensity reaches value ε_f, then the element loses its stiffness and is removed from the mesh. In this case the equation describing the

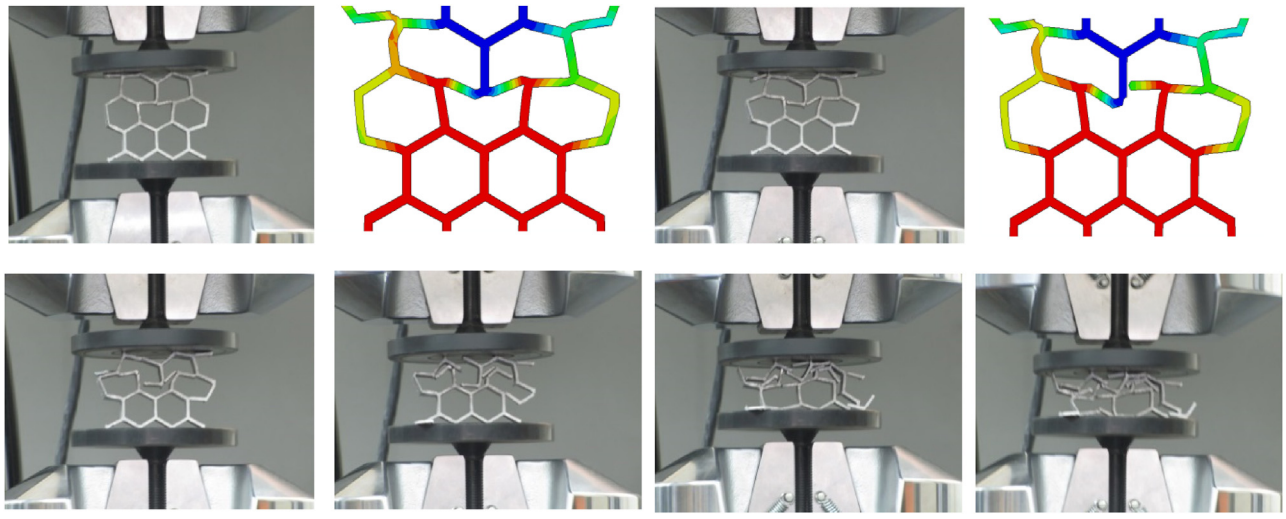

Fig. 8 – Comparison of deformation of the honeycomb structure manufactured from 4xxx.0 series alloy during testing on the MTS strength testing machine and the deformation during computer simulation.

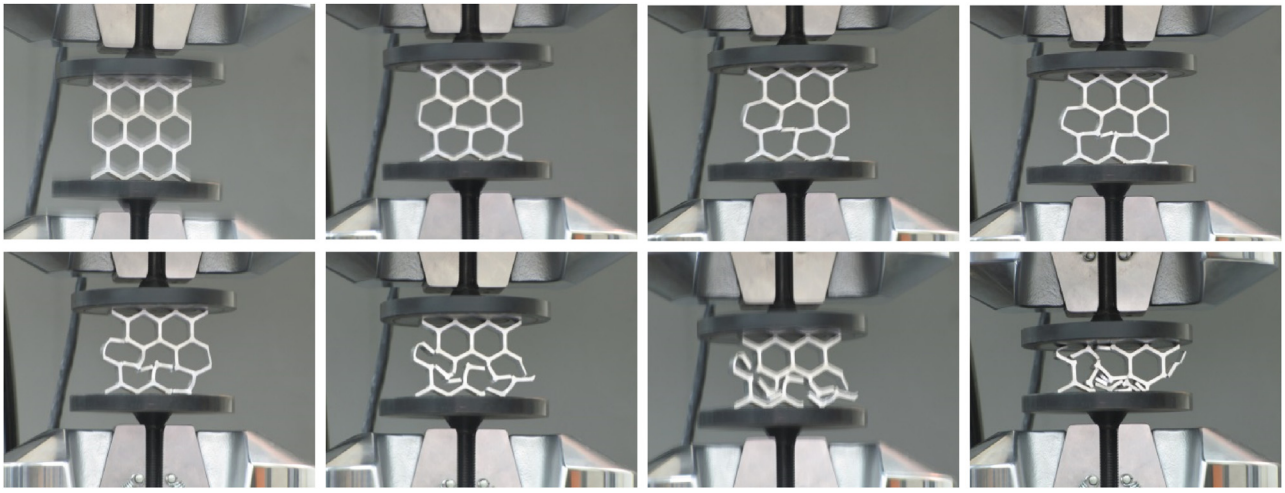

Fig. 9 – Deformation of the honeycomb structure manufactured from 4xxx series aluminium alloy on the CNC machining during compression on the MTS machine.

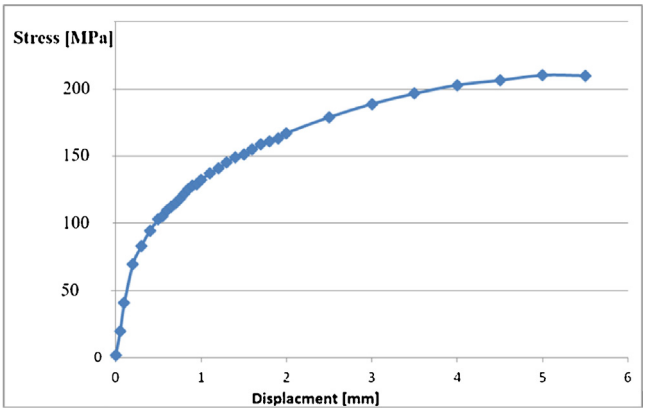

Fig. 10 – Tensile strength testing curve for the 4xxx.0 alloys used in the laboratory trials.

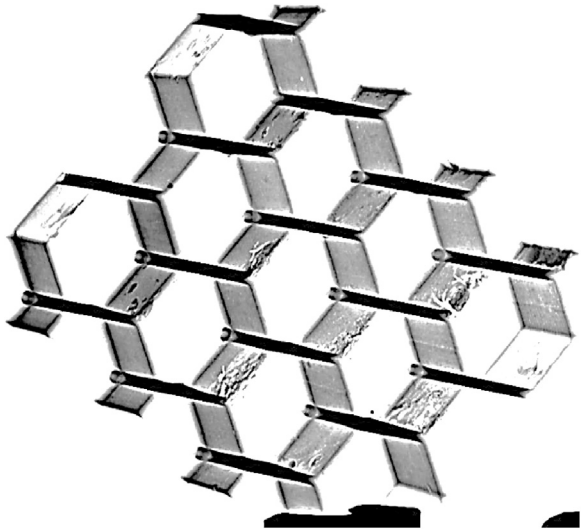

Fig. 11 – Visualization of internal defects of cast honeycomb cellular structure used in the laboratory trials.

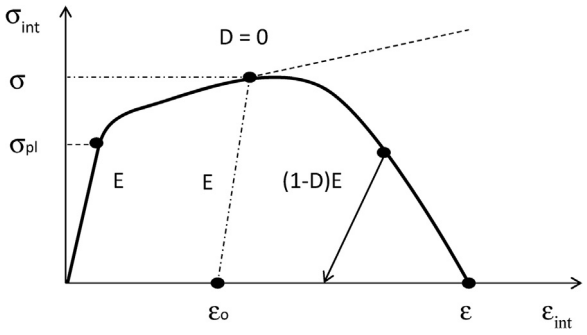

Fig. 12 – The tensile curve $\sigma = f(\varepsilon)$, with the progressive degradation of material stiffness.

destruction propagation expressed by the maximum displacement of the element which is a function of its deformation and the diagonal length of the element. In case where the material properties includes the internal porosities it is necessary to determine its percentage based on the simulation of solidification process or *NDT* inspection. The description of the material with internal porosities takes an isotropic nature of failure measured with a scalar variable. Based on the assumption that the defect is defined as a spherical void with increasing radius and non-homogenous density. Growth of these voids is not affected by the direction of maximum stress (tensile), but on the microstructure level, they turn to be responsible for the formation of microcrack and further failure propagation. The effect of the stress state on the speed of failure growth is taken isotropically by the triaxiality of the stress T_R. In addition, with the further growth of failure, in this case, the volume of the spherical void increases. All components of the stress tensor are updated and the reduced stress σ_o is calculated. The above assumption which describe the spherical character of voids in the elastic material was adopted in the model of failure propagation in the porous material, known as the Gurson model [15] and further generalized by Tvergaard and Needleman [16,17]. The elastic surface in this

case is described as the mean stress function σ_m, the stress intensity σ_{int} and current volume density of the void f^* [18]:

$$\phi(\sigma_{int},\sigma_m,f^*)=\frac{\sigma_{int}^2}{\sigma_{pl}^2}+2q_1f^*\cosh\left(\frac{-3q_2\sigma_m}{2\sigma_{pl}}\right)-1-(q_1f^*)^2=0 \quad (5)$$

where: q_1, q_2 – constant values introduced by the Tvergaard and Needleman, which in the basic Gurson model were ignored and $q_1 = q_2 = 1$. The σ_{pl} symbol is describing the actual yield strength of the material subjected to the isotropic hardening. The f^* function is defined as:

$$f^*=\begin{cases} f_V & dla \quad f_V\le f_{CR} \\ f_{CR}+\frac{f_u-f_{CR}}{f_F-f_{CR}}(f_V-f_{CR}) & dla \quad f_V>f_{CR} \end{cases} \quad (6)$$

f_{CR} – the critical value, which describes the mean volume density of the voids, upon which the individual voids merge, creating macrocracks carousing loss of stability. In the special case where there is no failure $f^* = f_V = 0$, the elastic function is reduced to the HMH criterion. The symbol f_F is the volume density in the moment of complete destruction and the $f_U = 1/q$.

The function described by Eq. (6) and its graphical interpretation (Fig. 13) shows that after reaching of the critical value f_{CR} a much quicker increase of the f^* function occurs. The A–B line shows the quick loss of stability compared to the basic Gurson model, which is presented as A–C line. The solution of the equation requires the determination of the constants q_1, q_2 and f_{CR}. Tvergaard' numerical calculation of the influence of many periodically spared voids suggested that the values of the constant were $q_1 = 1.5$; $q_2 = 1$. The critical value of the voids volume f_{CR} is not dependent, in the GT model on the degree of triaxiality stress state, but generally is assumed to be within the range of $f_{CR} = 0.05$ to $f_{CR} = 0.1$. It is assumed that the value is dependent on the material type and initial amount of voids.

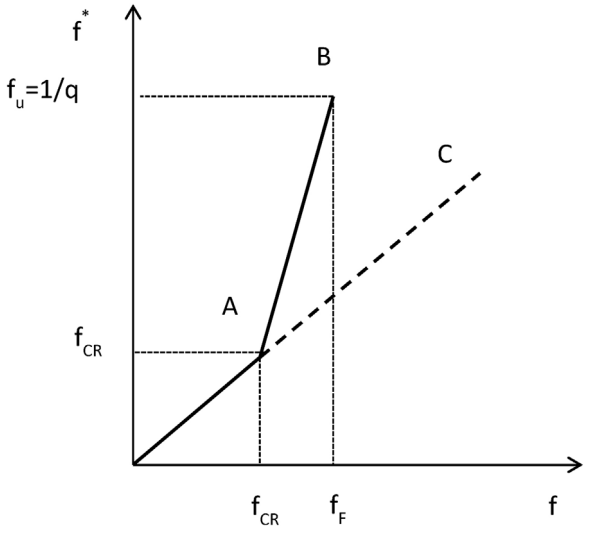

Fig. 13 – The graphic representation of Eq. (6).

6. The results of numerical calculations

The numerical analysis of the compression of the honeycomb cellular structure was based on the model presented in Fig. 14, which shows the reduced stress field according to the H–M–H hypothesis at the initial stage of the deformation.

As a result of the compression simulation the total energy absorbed by the cellular structure was calculated. The total energy includes the energies of: elastic deformation, plastic deformation and the energy dispersed by the friction between the surface of the model which have mechanical contact during deformation. Energy dissipation was also identified as a result of the destruction process. Changes of the amount of absorbed energy for the structure manufactured in the CNC and investment casting process are shown in Figs. 15 and 16. In Fig. 17 presented results are for the numerical modelling of the absorption of 7xxx.0 series Al alloy. In both cases, the results of

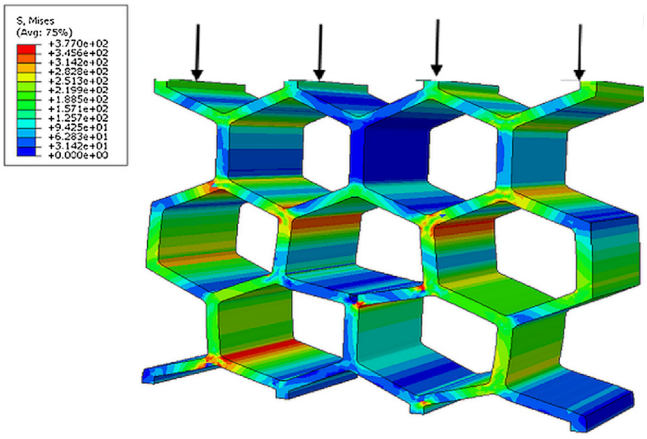

Fig. 14 – Reduced stress filed determined in the FEM method according to the HMH hypothesis at the initial stage of the deformation of the honeycomb structure. The arrows show the direction of applied force.

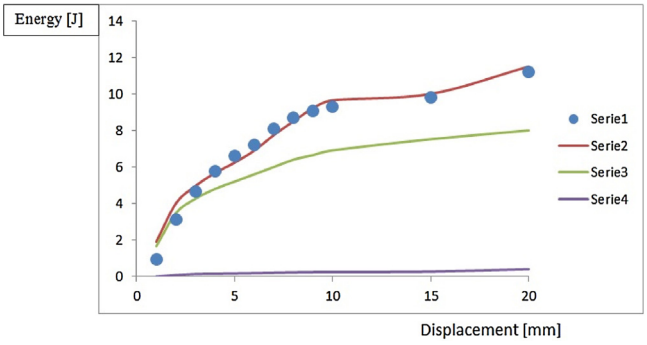

Fig. 15 – Energy absorption during the compression process by the honeycomb cellular structure manufactured from 4xxx.0 alloy in the investment casting process, determined experimentally and numerically, 1 – total energy determined experimentally, 2 – total energy determined by the numerical calculations, 3 – deformation energy determined by the numerical calculations, 4 – destruction energy determined by the numerical calculation,.

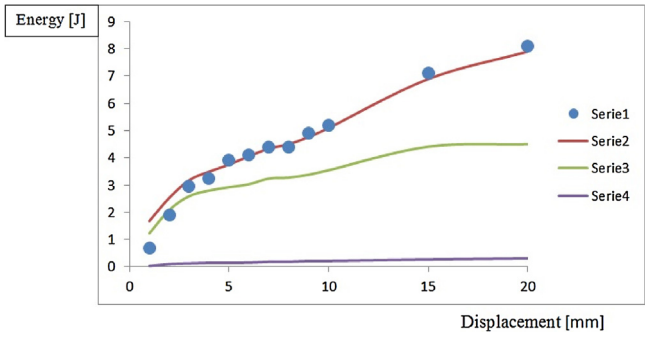

Fig. 16 – Energy absorption during the compression process by the honeycomb cellular structure manufactured from 4xxx.0 alloy in the investment casting process with detected porosity, determined experimentally and numerically, 1 – total energy determined experimentally, 2 – total energy determined by the numerical calculations, 3 – deformation energy determined by the numerical calculations, 4 – destruction energy determined by the numerical calculation,.

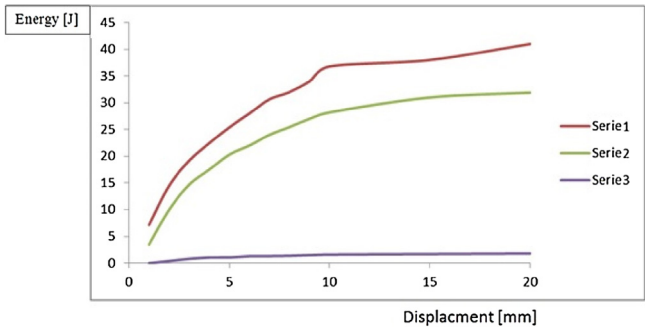

Fig. 17 – Energy absorption during the compression process by the honeycomb cellular structure manufactured from 7xxx.0 alloy in the CNC process, determined experimentally and numerically, 1 – total energy determined by the numerical calculations, 2 – deformation energy determined by the numerical calculations, 3 – destruction energy determined by the numerical calculation.

the numerical calculations have good correlation with the result of laboratory testing's. The result refers to changes in the total energy absorbed by the structure defined by MES analysis (series-2) and by the work performed by the external force, recorded during experimental trials (series-1).

Taking into account the possibility of occurrence of casting defects, the numerical calculation was also carried out including their presence. The effect of a defect in the structure is defined by its location, size and the constitutive material model in the occurrence area including the percentage of porosity. The energy changes during compression in numerical calculation were compared to the casting with detected internal porosity. The results are shown in Fig. 15.

7. Conclusions

The elements responsible for the energy absorption should have both high strength and deformability. The scope of the research work include the preparation of constitutive model based on the destruction testing of the material of which the honeycomb structure are manufactured in a single geometry the energy-absorbing thin-walled profiles and cellular structures may well meet the requirements for strength and deformability of such structures. Analysis of the structure including the internal porosities shows lower energy absorption. Forward-looking the use of investment casting and AM models as the technology of energy absorption is promising. The article presents the possibility of using the numerical modelling of deformation processes of cast cellular structures for the analysis of their energy absorption. Taking into account the nature of the casting technology the numerical model includes a constitutive description of porous material. Conducted laboratory experiments confirmed the rightness of using the AM method in the manufacturing of the cellular structure model and the final casting with good dimensional accuracy. A very good correlation between the numerical analysis and the experimental trial was observed. This confirms the correctness of the numerical model and is an accurate starting point for further analysis for different more complex shapes and different load conditions.

Ethical statement

Authors state that the research was conducted according to ethical standards.

Acknowledgements

This study was supported under AGH-UST research and development study no. 11.11.170.318.

REFERENCES

[1] E. du Maire, T. Schmidt, Bionik und Werkzeugmaschinenguss – ein wiederschpruch? Konstr. Giessen. 28 (2) (2003) 9–12.
[2] M. Cholewa, T. Szuter, Structure of AlSi skeleton castings, Arch. Foundry Eng. 12 (2) (2012) 147–152.
[3] M. Cholewa, T. Szuter, M. Dziuba, Basic properties of 3D cast skeleton structures, Arch. Mater. Sci. Eng. Process. 52 (2) (2011) 101–111.
[4] J. Piekło, S.S. Pysz, M. Małysza, Proces wykonania i mechaniczne właściwości odlewanych, uporządkowanych konstrukcji komórkowych ze stopu Al-Si, Prace Instyt. Odlewn. 1 (4) (2010) 17–29.
[5] M. Mazur, M. Leary, M. McMillan, J. Elambasseril, M. Brandt, SLM additive manufacture of H13 tool steel with conformal cooling and structural lattices, Rap. Protot. J. 22/3 (2016) 504–518L;ĆL. Valdevit, Z. Wei, C. Mercer, F.W. Zok, A.G. Evans, Structural performance of near-optimal sandwich panels with corrugated cores, Int. J. Solids Struct. 43 (2006) 4889–4905.

[6] S. Chiras, D.R. Mumm, A.G. Evans, N. Wicks, J.W. Hutchinson, K. Dharmasena, H.N.G. Wadley, S. Fichter, The structural performance of near-optimized truss core panels, Int. J. Solids Struct. 39 (2002) 4093–4115.
[7] J. Piekło, S. Pysz, M. Małysza, A. Karwiński, Analysis by numerical calculations of the depth and dynamics of the penetration of ordered cellular structure made by casting from AlSi10Mg eutectic alloy, Arch. Foundry Eng. 11 (3) (2011) 171–176.
[8] B. Hucko, L. Faria, Material model of metallic cellular solids, Comput. Struct. 62 (6) (1997) 1049–1057.
[9] L.J. Gibson, M.F. Ashby, Cellular Solids – Structure and Properties, Pergamon Press, Oxford, Toronto, 1987.
[10] N.G. Haydn, N.G. Wadley, Cell. Met. Manuf. Adv. Eng. Mater. 4 (10) (2002) 726–733.
[11] H.N.G. Wadley, N.A. Fleck, A.G. Evans, Fabrication and structural performance of periodic metal sandwich structures, Compos. Sci. Technol. 63 (2003) 2331–2343.
[12] M.M. Piekło, Methods of additive manufacturing used in the technology of skeleton castings, Arch. Metall. Mater. 59 (2) (2014) 699–702.
[13] L. Gołaski, Elements of Experimental Fracture Mechanics, Politechnika Świętokrzyska, Kielce, 1992 (in polish).
[14] Abaqus 6.14 Analysis User's Manual, Dassault Systemes, 2014.
[15] A.L. Gurson, Continuum theory of ductile rupture by void nucleation and growth, Part I – yield criteria and flow rules for porous ductile media, journal of engineering materials and technology, Trans. ASME 99 (1) (1997) 2–15.
[16] V. Tvergaard, Ductile fracture by cavity nucleation between larger voids, J. Mech. Phys. Solids 30 (1982) 265–286.
[17] V.V. Tvergaard, A.A. Needelman, Analysis of the cup-cone fracture in a round tensile bar, Acta Metall. 32 (1) (1984) 157–169.
[18] J. Skrzypek, Fundamentals of damage mechanical, Politechnika Krakowska, Kraków, 2006 (in polish).